https://doi.org/10.5194/egusphere-2026-6515
Preprint. Discussion started: 9 November 2026
© Author(s) 2026. CC BY 4.0 License.

Nitric oxide emissions from lakes in the Northern Hemisphere

Wanshan Tan[1], Jintai Lin[1,2,3*], Hao Kong[1], Mengying Wang[1], Sijie Wang[1], Yuhang Zhang[1], Lei Bai[4], Thomas Danckaert[5], Michel Van Roozendael[5], Yong Liu[6], Dianming Wu[7], Lian Feng[8], Xinming Wang[9], Xuejun Liu[10], Guiqian Tang[11], Kun Shi[12], Yunhua Chang[13], and Yujing Mu[14]

[1]Laboratory for Climate and Ocean-Atmosphere Studies, Department of Atmospheric and Oceanic Sciences, School of Physics, Peking University, Beijing, China

[2]Institute of Tibetan Plateau, Peking University, Beijing, China

[3]Institute of Carbon Neutrality, Peking University, Beijing, China

[4]Shanghai Artificial Intelligence Laboratory, Shanghai, China

[5] Royal Belgian Institute for Space Aeronomy (BIRA-IASB), Brussels, Belgium

[6]College of Environmental Sciences and Engineering, State Environmental Protection Key Laboratory of All Material Fluxes in River Ecosystems, Peking University, Beijing, China

[7]Key Laboratory of Geographic Information Science of the Ministry of Education, School of Geographic Sciences, East China Normal University, Shanghai, China

[8]State Key Laboratory of Information Engineering in Surveying, Mapping and Remote Sensing, Wuhan University, Wuhan, China

[9]State Key Laboratory of Advanced Environmental Technology and Guangdong Key Laboratory of Environmental Protection and Resources Utilization, Guangzhou Institute of Geochemistry, Chinese Academy of Sciences, Guangzhou, China

[10]State Key Laboratory of Nutrient Use and Management, College of Resources and Environmental Sciences, China Agricultural University, Beijing, China

[11]State Key Laboratory of Atmospheric Environment and Extreme Meteorology, Institute of Atmospheric Physics, Chinese Academy of Sciences, Beijing, China

[12]Key Laboratory of Lake and Watershed Science for Water Security, Nanjing Institute of Geography and Limnology, Chinese Academy of Sciences, Nanjing, China

[13]State Key Laboratory of Climate System Prediction and Risk Management, Nanjing University of Information Science and Technology, Nanjing, China

[14]Research Center for Eco-Environmental Sciences, Chinese Academy of Sciences, Beijing, China

*Correspondence to Jintai Lin (linjt@pku.edu.cn)

https://doi.org/10.5194/egusphere-2026-6515
Preprint. Discussion started: 9 November 2026
© Author(s) 2026. CC BY 4.0 License.



Abstract

Nitrogen oxides ($NO_x = NO + NO_2$) are a key player in the nitrogen cycle affecting health and climate. Recent work revealed high nitric oxide (NO) emissions from natural lakes on the Tibetan Plateau, yet the global prevalence and importance of lake emissions remain unclear. Here, we quantify NO emissions from 300 large natural or human-influenced lakes across the Northern Hemisphere (NH) in 2018–2024 summertime early afternoon, based on satellite measurements of tropospheric nitrogen dioxide (NO_2) and an advanced emission inversion algorithm. The average lake emission intensity reaches 0.15 ± 0.32 kg N km^{-2} h^{-1}, nearly four times greater than summertime soil emission intensity from croplands in the NH. The total emissions from all lakes amount to 70.95 ± 13.98 Tons N h^{-1}, equivalent to twice the anthropogenic emissions in Japan or nearly half of power-sector emissions in China. Emissions from many lakes are each comparable to anthropogenic emissions in global economic hub cities. Such considerable emissions across the NH lakes are either missing (for natural sources) or poorly represented (for anthropogenic sources) in current emission datasets and models. The significance of lake NO emissions calls for improved in-situ measurements and numerical models to better understand such lake-atmosphere interactions and their eco-environmental impacts.

https://doi.org/10.5194/egusphere-2026-6515
Preprint. Discussion started: 9 November 2026
© Author(s) 2026. CC BY 4.0 License.

1 Introduction

Lakes (including reservoirs) occupy about 3×10^6 km^2 of the Earth surface, and most of them are located in the Northern Hemisphere (NH) (Messager et al., 2016; Pi et al., 2022). Lakes are home to numerous microorganisms and planktons (Clark et al., 2018; Liu et al., 2015; Savvichev et al., 2018), which can decompose organic matter in the water and sediments through aerobic or anaerobic processes to produce carbon dioxide (CO_2) (Duarte and Prairie, 2005) and methane (CH_4) (Liu and Whitman, 2008). In addition, nitrification and denitrification processes in lakes can produce nitrous oxide (N_2O) (Soued et al., 2015). Emissions of these greenhouse gases (GHGs) are affected by lake environmental factors such as water temperature, chlorophyll-a (Chl-a) concentration, dissolved oxygen (DO), nitrogen and phosphorus contents (Beaulieu et al., 2019; DelSontro et al., 2018; Marotta et al., 2014; Yang et al., 2025; Zhou et al., 2021). The total emissions from global lakes amount to about 0.32 Pg C yr^{-1} for CO_2 (Raymond et al., 2013), 42 Tg yr^{-1} for CH_4 (Johnson et al., 2022) and 65 Gg N yr^{-1} for N_2O (Li et al., 2024) in recent decades. Yet lakes might also be an important source of tropospheric nitrogen oxides ($NO_x = NO + NO_2$) (Kong et al., 2023), which has largely been overlooked.

As a key player in the nitrogen cycle besides N_2O, NO_x affect human health, ecosystems and climate. NO_x are emitted mainly as nitric oxide (NO), and subsequently undergo chemical reactions in the atmosphere, resulting in being mainly in the form of nitrogen dioxide (NO_2). Yet the quantities of NO emissions from anthropogenic and natural sources remain highly uncertain (Weng et al., 2020; Zhao et al., 2011). Many lakes are influenced by local human activities such as shipping, but the existing bottom-up anthropogenic emission inventories (e.g., the Emissions Database for Global Atmospheric Research (EDGAR) (Crippa et al., 2024), the Community Emissions Data System (CEDS) (Hoesly et al., 2018), the Global Emission Modeling System (GEMS) (Huang et al., 2017) and the National Emissions Inventory (NEI) (Eyth et al., 2025)) contain large uncertainty in NO emissions from lakes. This is because the shipping data over inland lakes are not reliable (Crippa et al., 2024), with many fishing, transport and energy vessels missing from public datasets (Paolo et al., 2024) used in these inventories. Aquaculture might also lead to NO emissions (Preena et al., 2021) but are not included in these inventories. Several widely-used emission inventories do not include any emissions on lakes (e.g., the Multi-resolution Emission Inventory (MEIC) (Li et al., 2017) and the Regional Emission Inventory in Asia (REAS) (Kurokawa and Ohara, 2020)). Moreover, natural NO emissions from water were traditionally thought to be negligible, with an assumption that NO produced by microorganisms in water are consumed quickly before being released into the atmosphere (Tian et al., 2019). As a result, current emission datasets and climate and air quality models do not consider natural NO emissions from lakes (Byun and Schere, 2006; Dunne et al., 2020; Guenther et al., 2012).

However, recent satellite-based work (Kong et al., 2023) revealed many hotspots of tropospheric NO_2 vertical column densities (VCDs) over natural lakes on the Tibetan Plateau in summer 2019. The subsequently quantified NO emissions from 135 lakes

https://doi.org/10.5194/egusphere-2026-6515
Preprint. Discussion started: 9 November 2026
© Author(s) 2026. CC BY 4.0 License.

larger than 50 km^2 in size amount to 1.89 ± 0.54 Tons N h^{-1}, which are comparable to anthropogenic emissions in several megacities such as Beijing, New York City and London (Kong et al., 2023). In addition, a field study of three lakes on the Yunnan Plateau in southwestern China in summer 2022 detected a large amount of NO in surface water related to microbial activity (Chen et al., 2025), which were approximately two orders of magnitude higher than summer surface-water N_2O concentrations in two other Chinese reservoirs (Xiao et al., 2019; Yang et al., 2023b), and these NO could be further released into the atmosphere. In situ measurements also showed that NO_2 concentrations over several lakes were comparable to, or even higher than those over surrounding lands (Donaldson, 2026; Kong et al., 2024; Stanier et al., 2021). Together, these studies suggest that lakes are important sources of NO. Yet, their results are sparse in space and/or time, and thus the significance of lake NO emissions from both anthropogenic and natural sources on the global scale remains unknown.

In this study, we analyze the seasonal variation of NO_2 VCDs and then quantify summertime (June, July and August) NO emissions from 300 large lakes (> 200 km^2) in the NH during 2018–2024, based on satellite NO_2 VCDs data and a physics-based emission inversion algorithm (Peking university High-resolution Lifetime-Emission-Transport, PHLET) (Kong et al., 2022) with a resolution of 0.05° × 0.05°. These 300 lakes are located in five continents, covering 6.7 × 10^5 km^2 in total; see Supplementary Data for geolocation and other details. They are classified into 102 natural lakes away from human activities and 198 human-influenced lakes, based on multiple anthropogenic activity datasets. To ensure the quality of lake NO_2 VCDs, we exclude satellite pixels with unphysical, negative retrieved water vapor concentrations or affected by sun glint, in addition to adopting the commonly used filtering criteria. The PHLET algorithm quantifies NO emissions from NO_2 VCDs under the influences of meteorology-driven horizontal transport and nonlinear chemistry (Kong et al., 2022), and it exhibits high accuracy in different countries. Given the satellite overpass time, the VCDs and emissions represent the early-afternoon values. We find that considerable NO emissions are released from these lakes across the vast NH, providing spaceborne evidence of previously missed or poorly-represented sources of this important pollutant from a vital ecosystem that should be included/enhanced in future environmental analyses and modeling.

2 Materials and Methods

2.1 Tropospheric NO_2 VCDs from satellite

The Tropospheric Monitoring Instrument (TROPOMI) is aboard the Sentinel-5 Precursor satellite launched in October 2017, and it crosses the equator at 13:30 local solar time (LST) (Veefkind et al., 2012). TROPOMI offers unprecedented high-resolution global NO_2 monitoring, with a pixel size of about 7 km × 3.5 km at nadir, which was refined to about 5.5 km × 3.5 km since August 2019.

Here, we use the official TM5-MP-DOMINO Level 2 NO_2 product (S5P-RPRO for 2018–2021, and S5P-OFFL for 2022–2024) to derive monthly and summertime NO_2 VCDs. For Asia (70°–140° E, 15°–55° N), we adopt the POMINO-TROPOMI (Liu et

https://doi.org/10.5194/egusphere-2026-6515
Preprint. Discussion started: 9 November 2026
© Author(s) 2026. CC BY 4.0 License.

al., 2020) v1.2.2 Level 2 product with enhanced data quality, for all months in 2018–2022 and summer months (June–August) in 2023 and 2024 given the data availability. The POMINO-TROPOMI algorithm uses the tropospheric slant column densities (SCDs) data from the official product but recalculates the air mass factors to derive NO_2 columns. Compared to the official product, POMINO-TROPOMI explicitly accounts for the effects of aerosol scattering and absorption and surface reflectance anisotropy, and employs a priori NO_2 vertical profiles with a higher horizontal resolution (25 km versus 100 km). Therefore, it shows a smaller bias of NO_2 VCDs relative to ground-based MAX-DOAS measurements (Liu et al., 2020).

We calculate gridded NO_2 VCDs data at $0.05° \times 0.05°$ resolution from the Level 2 data. For this purpose, we select satellite pixels that satisfy all of the following criteria: QA_value $\geq$ 0.75 for the official product; and QA_value $\geq$ 0.5, CRF $\leq$ 0.5, solar zenith angle (SZA) $\leq$ 80°, viewing zenith angle (VZA) $\leq$ 80°, no icy or snowy ground, surface blue-sky albedo $\leq$ 0.3, and AOD $\leq$ 3 for POMINO-TROPOMI. The above screening is commonly used and is referred to here as Screening 1.

We further remove pixels over lake water that might be affected by sun glint under specific satellite-Sun geometries and result in abnormally high surface albedo and bright satellite true-color images (Kay et al., 2009). Specifically, we only select pixels without sun glint warning, i.e., bit 11 in the processing_quality_flags is set to "1", which excludes 11 % of the pixels after Screening 1. This screening is referred to as Screening 2.

Furthermore, for some lake pixels, the spectral fit to obtain NO_2 SCDs can lead to low-frequency residuals (wavelength > 10 nm) in the 430–460 nm range, accompanied with unphysical, negative retrieved water vapor (H_2O) SCDs (Labzovskii et al., 2024). More recently, van Geffen et al. (2026) identified a prominent residual feature around 430 nm associated with the omission of vibrational Raman scattering (VRS) over water pixels. Because VRS cannot currently be explicitly accounted for in NO_2 SCD retrievals, they introduced a NO_2-gap approach in which wavelengths between 428 and 433 nm are excluded from the DOAS-based NO_2 SCD retrieval. Here, we use a Python version of the open-source code of QDOAS (Fayt et al., 2026) to conduct both full-window and NO_2-gap retrievals in August 2019, and retain the pixels meeting the two screening criteria described above. The Python version of QDOAS reproduces the NO_2 SCD fitting results by the original QDOAS (written in C++) when all input data are kept the same (i.e., r = 1.00, NMB = 0.00 %, linear regression slope = 1.00, and intercept = 0.00, with a relative difference within 5×10^{-4} % for any given pixel globally, based a test on 1 August 2019). Across the 300 lakes, the mean normalized difference between NO_2-gap and full-window retrievals is 1.7 % (5th–95th percentile: 0.4 % to 2.9 %). This small difference suggests that the fitting residual feature around 430 nm has a limited overall impact on lake NO_2 SCDs.

We further examine whether the over-lake Ring effect coefficients fitted alongside the SCDs are affected by the low-level fitting residuals, as another indicator of potential failure in lake NO_2 SCD fitting. For this purpose, we compare the QDOAS-fitted Ring effect coefficients over individual lakes (from grid cells with the areal proportion of lake water exceeding 90%) with those over its surrounding (within 4 non-lake grid cells

https://doi.org/10.5194/egusphere-2026-6515
Preprint. Discussion started: 9 November 2026
© Author(s) 2026. CC BY 4.0 License.

of the lake periphery). Only pixels with QA ≥ 0.75 and without sun glint warning are included. This results in generally similar values of fitted Ring effect coefficient for lake and its surrounding globally, with a median relative difference of 4.67 % (Figure S1a–c). Zoomed-in results over the Tibetan Plateau also show no systematic lake–surrounding differences across the lakes (Figure S1d).

The NO_2-gap approach cannot eliminate the low-frequency structures in the fitting residuals at wavelengths above 433 nm. Since the KNMI's official SCD product does not provide data for spectral fitting residuals, we further use negative values of retrieved H_2O SCDs as the indication of such abnormal fitting, and only select lake pixels with positive H_2O SCDs. This screening is referred to as Screening 3.

To ensure the proper use of Screening 3, we quantitatively examine whether the exclusion of lake pixels with negative retrieved H_2O SCDs can effectively remove the effect of low-frequency fitting residuals in 430–460 nm, based on a test in summer 2019. First, we use the QDOAS model (Fayt et al., 2026) to conduct full-window spectral fitting, and obtain the fitting residuals and H_2O SCDs for each pixel of each orbit. We then assess the existence of low-frequency variability by applying a discrete Fourier transform to the 430–460 nm fitting residuals for each pixel. In the Fourier transform (Eqs. (1)–(3)), $x(t)$ $(t = 1,2, \dots, n, n = 152)$ denotes the fitting residuals with the sampling interval of 0.2 nm, k the wavenumber, and a_k and b_k the Fourier coefficients. Subsequently, the F statistic is used to evaluate the significance of low-frequency harmonics ($k = 1–3$, corresponding to the wavelength of the low-frequency feature > 10 nm; Eq. (4)); here, the variance of $x(t)$ is denoted by s^2, the variance of the harmonic with wavenumber k is denoted by $\frac{1}{2}(a_k^2 + b_k^2)$, the numerator degrees of freedom is 6, and the denominator degrees of freedom is $n - 6 - 1$. At the 1 % significance level ($\alpha = 1\,\%$), the threshold value F_α is 3, indicating that low-frequency variability is statistically significant when F exceeds 3. The test results for all lake pixels show that, among the pixels with negative H_2O SCDs (that are removed), 59 % exhibit low-frequency fitting residuals at the 1 % significance level, with the rest 41 % pixels being associated with other imperfections in spectral fitting. By comparison, for the lake pixels with positive H_2O SCDs, only 4 % exhibit low-frequency fitting residuals, and further removing these low-frequency pixels has a negligible impact on the lake NO_2 VCDs (by -2.0 % to 0.6 %, 5th–95th percentile). Even at the 5 % significance level ($F_\alpha = 2.2$, which leads to more pixels being considered to have low-frequency residuals), 11 % of pixels with positive H_2O SCDs exhibit low-frequency residuals, but their impact on lake NO_2 VCDs is still very small (by -2.2 % to 1.1 %, 5th–95th percentile). Therefore, excluding lake pixels with negative H_2O SCDs represents a practical, effective method to remove lake pixels affected by low-frequency fitting residuals.

$$x(t) = a_0 + \sum_{k=1}(a_k \cos \omega_k t + b_k \sin \omega_k t), \text{ k=1,2,…,76 } (n/2) \quad (1)$$

$$a_k = \frac{2}{n} \sum_{t=1}^{n} x_t \cos \frac{2\pi k}{n}(t-1) \quad (2)$$

$$b_k = \frac{2}{n} \sum_{t=1}^{n} x_t \sin \frac{2\pi k}{n}(t-1) \quad (3)$$

https://doi.org/10.5194/egusphere-2026-6515
Preprint. Discussion started: 9 November 2026
© Author(s) 2026. CC BY 4.0 License.

$$F = \frac{\frac{1}{2}\sum_{k=1}^{3}(a_k^2+b_k^2)/6}{(s^2-\frac{1}{2}\sum_{k=1}^{3}(a_k^2+b_k^2))/(n-6-1)} \quad (4)$$

After applying Screening 2 and 3, the summer average NO_2 VCDs over 2018–2024 decrease by more than 10 % over 8 out of the 41 lakes (including 38 natural and 3 human-influenced) on the Tibetan Plateau, but they are still 1.2–1.3 times the VCDs over their surroundings (Table S1). In other TP lakes, the relative changes of NO_2 VCDs range from -8 % to 2 %. And for lakes in other regions, the relative changes range from -6 % to 7 % (Figure S2). For 98 % of lakes on the Tibetan Plateau and 72 % of lakes in other regions, NO_2 VCDs over lakes are higher than those over their surroundings (Figure S3), compared with 98 % and 70 % before Screening 2 and 3 are applied. Overall, the above results suggest that Screening 2 and 3 have minor impacts on the NO_2 VCDs data and subsequent emission estimate on the hemispheric scale.

2.2 Comparison of in situ and satellite observations of NO_2 over or near lakes

There are very few in situ measurements of NO_x concentrations or fluxes over lakes. Based on the literature search, we obtain in situ measurements of tropospheric or near-surface NO_2 concentrations over or near four lakes over North America and Asia, and use them for independent validation of satellite data (Table S2). In situ and satellite data are matched spatially and temporally. For comparison with in situ measurements of near-surface NO_2, satellite NO_2 VCDs are converted to surface mixing ratios following previous work (Wang et al., 2026; Zhang et al., 2023).

Three lakes are human-influenced, with in situ measurements using shipborne or airborne instruments from Donaldson (2026) (for Lake Ontario) and Stanier et al. (2021) (for Lake Michigan), or as unpublished work by the authors (for Lake Taihu). Overall, in situ NO_2 concentrations are 1–3 times higher than those derived from TROPOMI. This suggests that TROPOMI data likely provide a low bound of NO_2 concentrations for these human-influenced lakes, although the differences in measurement methods (point measurements for in situ versus areal measurements for satellite) might also affect the comparison.

For natural lakes, to our best knowledge, there are almost no in situ measurements of NO_x, albeit with many measurements of GHGs. Based on measurements on the bank of Lake Nam Co on the Tibetan Plateau (Kong et al., 2024), near-surface NO_2 concentration shows a distinct diurnal pattern with a nighttime minimum and afternoon peak, indicating the dominant source from natural emissions. Moreover, during the satellite overpass time, prevailing winds blow from the lake toward the observation site (Figure S4), with in situ measured NO_2 mixing ratios reaching 2.6 ppb, comparable to TROPOMI-derived results (2.0 ppb). These results support the existence of high NO emission from Lake Nam Co.

2.3 NO emission inversion and uncertainty

We apply the physics-based PHLET model and its adjoint (Kong et al., 2022) to quantify NO emissions on a 0.05° × 0.05° grid based on the above-selected NO_2 VCDs data in the summers from 2018 to 2024. As detailed in Kong et al. (2022), PHLET is a two-dimensional (2-D) model that describes the relationship between NO emissions

https://doi.org/10.5194/egusphere-2026-6515
Preprint. Discussion started: 9 November 2026
© Author(s) 2026. CC BY 4.0 License.

and de-backgrounded NO_2 VCDs over a period of time (summer in this study). It incorporates the nonlinear chemistry, flux divergence caused by temporal average winds, and "effective" diffusion of NO_2 caused by the temporal deviations of wind speed. The de-background process removes the impact of NO_2 in the free troposphere (quantified as the 1 % percentile of NO_2 VCDs within 500 km of each grid cell, followed by a spatial smoothing to remove potential noise), and it allows the de-backgrounded NO_2 VCDs to be more closely tied to surface emissions. PHLET has been used to investigate anthropogenic emissions in China (Kong et al., 2022) and natural lake emissions on the Tibetan Plateau (Kong et al., 2023).

This study improves PHLET by using the European Center for Medium Weather Forecasting (ECMWF) real-time analysis wind field data with a higher horizontal resolution of 9 km, compared with previous wind data from GEOS-FP at 0.25° (lat) × 0.3125° (lon) resolution. This higher-resolution wind field data can more accurately depict the wind field in complex terrains and the local atmospheric circulation between lakes and surrounding land. We regrid the wind fields at different pressure levels to 0.05° × 0.05° by bi-linear interpolation, calculate the vertical average wind from the surface to 500 m, and then linearly interpolate the data to 13:30 LST to match the satellite overpass time.

To quantify the uncertainty (1-σ) of PHLET inversion, a 20-member Monte Carlo experiment is conducted. The experiment accounts for uncertainties from satellite NO_2 VCDs, background removal, steady-state assumption, meteorological data, NO_2 lifetime, NO_2-to-NO_x ratio and other procedures, as described in previous work (Kong et al., 2022). For each grid cell, the NO_2 VCD uncertainty is taken to be 20 % + 0.5 × 10^{15} molecules cm^{-2}, with equal contributions from systematic and random errors.

2.4 Validation of PHLET-derived emissions

Previous work has assessed the reliability of PHLET. For China, the PHLET-derived anthropogenic NO emissions are within 15 % of each of four bottom-up anthropogenic emission inventories at the national level, but PHLET reveals much finer emission details at the local scale, including a considerable number of small sources, substantial cross-city disparity in emission trends, and emission changes associated with power plant dynamics (close-down and built-up) which are missing from these inventories but confirmed by independent datasets (Kong et al., 2022; Kong et al., 2025; Xu et al., 2026). Over the Tibetan Plateau, the PHLET-derived emissions from natural lakes are also supported by in situ measurements of near-surface concentrations (Kong et al., 2024).

Here we further validate the applicability of PHLET to other regions, by applying PHLET to estimate emissions in the Contiguous United States (CONUS) and comparing the PHLET-derived anthropogenic emissions (by subtracting fire and soil emissions from the PHLET-derived total emission and excluding the grid cells with no human activities, following Kong et al. (2022)) with the NEI. The NEI provides monthly average hourly gridded (0.1° × 0.1°) NO emissions in 2022 (Eyth et al., 2025). To ensure a temporally consistent comparison, we calculate NEI emissions for summer

https://doi.org/10.5194/egusphere-2026-6515
Preprint. Discussion started: 9 November 2026
© Author(s) 2026. CC BY 4.0 License.

early-afternoon (LST 13:00–14:00). We find that PHLET anthropogenic NO emissions are about 298 ± 75 Tons N h^{-1} in the CONUS in summer 2022 early afternoon, which are approximately 4 % lower than NEI (312 Tons N h^{-1}), with a strong spatial correlation of 0.89 at the state level, or 0.92 when the outlier data point for California is excluded (Figure S5). This comparison further supports the general reliability of PHLET-derived emissions.

2.5 Selection and classification of lakes

We use two datasets of lake shapefile to generate lake masks, including the Reservoir and Lake Surface Area Timeseries (ReaLSAT) (Khandelwal et al., 2022) and the HydroLAKES (Messager et al., 2016). ReaLSAT provides monthly shape of lakes larger than 0.1 km^2 in 60° S–50° N from 1984 to 2020, with a resolution of 1 arc-second (~30 m at the equator). HydroLAKES provides static shapes of global lakes larger than 0.1 km^2, at the same resolution as ReaLSAT in our research domain. We regrid lake shape data of ReaLSAT (0°–50° N) and HydroLAKES (50° N–60° N) to both 0.01° × 0.01° and 0.05° × 0.05° grids. If the center of a 0.01° grid cell is located in a lake, we mark this grid cell as lake. Then, we calculate the proportion of lake area in a 0.05° grid cell based on the number of 0.01° lake grid cells inside that 0.05° grid cell.

Considering the horizontal resolution of PHLET (~25 km^2 per grid cell), we focus on large lakes with area larger than 200 km^2 and completely covering at least one 0.05° grid cell, to ensure sufficient grid coverage over the lakes. In addition, we remove nine irregularly-shaped lakes (Figure S6) for which it is difficult to distinguish emissions from lakes and those from their surrounding land. To further reduce uncertainty, we require that in a given lake, more than one third of its 0.05° grid cells have non-zero emissions for at least six years during 2018–2024. This criterion removes 54 lakes. At last, we obtain 300 large lakes in the NH to be analyzed in the main text.

Human activities, such as aquaculture and industry, can alter the biochemistry of lakes, which may in turn affect NO emissions from lakes. Thus, we classify the 300 lakes into 198 human-influenced lakes and 102 natural lakes based on population density data from Worldpop (WorldPop and Center for International Earth Science Information Network (CIESIN), 2018), AIS ship density (Cerdeiro et al., 2020), aquacultural data derived from Sentinel-2 satellite image (Wang et al., 2022b), and anthropogenic point-source facility data from the Global Energy Monitor (GEM), including combustion-based power plants, heavy industry and fossil fuel extraction facilities (Global Energy Monitor, 2026a, b, c, d, e). Specifically, a lake is classified as human-influenced lake if it meets any of the following criteria: the average population density within 20 km (i.e., the length of four 0.05° grid cells) of its periphery exceeds 10 km^{-2}, the maximum population density within 10 km exceeds 100 km^{-2}, the maximum population density within 20 km exceeds 200 km^{-2}, the maximum population density within 50 km exceeds 1000 km^{-2} , the ship density over the lake exceeds zero, aquacultural activity is present within the lake, or at least one anthropogenic facility is located within 10 km of its periphery. Otherwise, the lake is classified as natural lake.

2.6 Calculation of monthly NO_2 VCDs over lakes and surroundings

https://doi.org/10.5194/egusphere-2026-6515
Preprint. Discussion started: 9 November 2026
© Author(s) 2026. CC BY 4.0 License.

We calculate monthly mean NO_2 VCDs over 300 lakes and their surrounding areas from May 2018 to December 2024, which are defined as follows.

$$VCD_{lake_x} = \frac{\sum_{i=1}^{n} VCD_{i,x} \times lake_ratio_{i,x} \times area_{i,x}}{\sum_{i=1}^{n} lake_ratio_{i,x} \times area_{i,x}} \quad (5)$$

$$VCD_{sur_x} = \frac{\sum_{i=1}^{m} VCD_{i,x} \times sur_ratio_{i,x} \times area_{i,x}}{\sum_{i=1}^{m} sur_ratio_{i,x} \times area_{i,x}} \quad (6)$$

For lake x, $lake_ratio_{i,x}$ denotes the fraction of the 0.05° grid cell i covered by lake x; and $sur_ratio_{i,x}$ denotes the fraction of i not covered by any lakes. n denotes the number of 0.05° grid cells with $lake_ratio_{i,x} > 0$, population density < 10 km^{-2}, and the number of anthropogenic point-source facilities = 0. m denotes the number of surrounding grid cells within 20 km (four 0.05° grid cells) of the periphery of lake x. As such, the surrounding could include a few grid cells with anthropogenic and/or open-fire emissions; and excluding these human- or fire-influenced surrounding grid cells increases the lake–surrounding VCD difference very slightly. $area_{i,x}$ denotes the area (in km^2) of i. If more than half of the grid cells in a lake or its surrounding area have missing NO_2 VCD values in a given month, the data for that lake in that month are removed; this situation occurs in winter for 71 natural lakes and 50 human-influenced lakes.

2.7 Derivation of lake emission intensities and total emission amounts

Some grid cells on the lake-land boundary area might be affected by open fires, resulting in elevated NO emissions. To exclude the effect of fires along lake shorelines, PHLET-derived emissions are subtracted by the maximum values of fire emissions among three datasets at 0.1° × 0.1° resolution, and are subsequently used in the following calculations. These fire datasets include the Fire INventory (FINN v2.5) (Wiedinmyer et al., 2023), the Quick Fire Emissions Dataset (QFED v2.6r1) (Darmenov and Silva, 2015), and the Global Fire Assimilation System (GFAS v1.2) (Kaiser et al., 2012).

The emission intensities and total emissions from lakes in summer are calculated according to Eqs. (7) and (8).

$$E_{ave,x,y} = \frac{\sum_{i=1}^{n} e_{i,x,y} \times lake_ratio_{i,x} \times area_{i,x}}{\sum_{i=1}^{n} lake_ratio_{i,x} \times area_{i,x}} \quad (7)$$

$$E_{tot,x,y} = E_{ave,x,y} \times \sum_{i=1}^{p} (lake_ratio_{i,x} \times area_{i,x}) \quad (8)$$

Here, y denotes the year and x the lake. $e_{i,x,y}$ denotes PHLET-calculated summertime NO emission intensity (kg N km^{-2} h^{-1}) in the 0.05° grid cell i of lake x for year y. $lake_ratio_{i,x}$, $area_{i,x}$ and n are defined in Eqs. (5) and (6). p denotes the total number of 0.05° grid cells covered by lake x ($lake_ratio_{i,x} > 0$). $E_{ave,x,y}$ denotes the average emission intensity of lake x in year y. For human-influenced lakes, $E_{ave,x,y}$ excludes the residential and point-source anthropogenic emissions in lake-land boundary area (because n excludes grid cells with population density greater than 10 km^{-2} or point-source facilities), but may include anthropogenic emissions on lakes such as shipping, tourism, and aquaculture. $E_{tot,x,y}$ (kg N h^{-1}) denotes the emission amount, which is calculated as the lake-average emission intensity $E_{ave,x,y}$ multiplied by lake total area.

https://doi.org/10.5194/egusphere-2026-6515
Preprint. Discussion started: 9 November 2026
© Author(s) 2026. CC BY 4.0 License.

For quality control, in a given year, if less than one third of 0.05° grid cells in a lake have non-zeros emissions, we remove emissions from that lake in that year. Then for each lake, we calculate the multi-year average of $E_{ave,x,y}$ and $E_{tot,x,y}$ to obtain more representative values of emission intensity ($E_{ave,x}$) and total emission ($E_{tot,x}$), which are analyzed in the main text.

2.8 Sensitivity test by using only lake-interior grid cells

To assess the potential influence of anthropogenic and open-fire emissions near lake shorelines and lake-land mixed grid cells on our results, we recalculate lake-level NO_2 VCDs and NO emissions using a conservative lake-interior grid cell selection scheme as a sensitivity analysis. The lake grid cells are selected according to the following two criteria. First, a grid cell is retained only if the grid cell itself and all eight neighboring grid cells belong to the same lake ($lake_ratio > 0$), thereby removing the outermost ring of 0.05° lake grid cells. Second, the retained grid cells are required to be entirely covered by lake ($lake_ratio = 1$). Together, these criteria retained only lake-interior grid cells away from the mapped shoreline. Examples of the lake-interior grid cells are marked with black crosses in Figures S7 d–f and S8 d–f. After applying both criteria, 98 natural lakes and 177 human-influenced lakes have at least one valid grid cell and are included in the sensitivity analysis.

2.9 Environmental factors of lakes and surroundings

We select two environmental factors with data available for global lakes. Summertime lake mixed-layer temperature data are taken from the ERA5-Land reanalysis (Muñoz Sabater, 2019) monthly dataset at a horizontal resolution of 0.1° for 2018–2024. Annual lake-average DO concentrations for 2003–2023 are obtained from Zhang et al. (2025), which are based on machine learning-aided extension of in situ measurements. For these two factors, multi-year mean values are used in the main text.

In situ measurement data of TN, TP and Chl-a concentrations in lakes are obtained from Naderian et al. (2024), who compiled and integrated data from accessible repositories, published articles, publicly available maps, as well as private and governmental reports up to 2022. Most measurements are located in human-influenced lakes. Here, we select measurements in May–September (rather than June–August, to obtain more data) for the period 2000–2022 and then project the data to 0.05° × 0.05°. For each grid cell, the concentration is defined as the mean of all measurement data within that grid cell. To better exclude the direct anthropogenic sources such as ship emissions, we remove grid cells with population density greater than 10 km^{-2}, or ship density (Cerdeiro et al., 2020) greater than zero, or aquacultural activity (Wang et al., 2022b). After the screening, we obtain in situ measurements of TN, TP and Chl-a in 35 (15), 40 (15), 183 (35) grid cells (lakes), respectively. In relating these factors and NO emissions, we apply logarithmic transformation following previous work on GHG emissions (DelSontro et al., 2018; Yang et al., 2025).

3 Results and Discussion

https://doi.org/10.5194/egusphere-2026-6515
Preprint. Discussion started: 9 November 2026
© Author(s) 2026. CC BY 4.0 License.

3.1 Seasonal variation of NO_2 VCDs over lakes and surroundings

Figure 1 shows the monthly mean early-afternoon NO_2 VCDs over the 300 lakes and their surrounding areas within 20 km of their peripheries in 2018–2024 (Sect. 2.6). The mean and median NO_2 VCDs over natural lakes and human-influenced lakes for each season are shown in Tables S3 and S4, respectively. Over natural lakes, NO_2 VCDs start to increase in spring, peak in summer, and then decrease until a minimum in winter (Figure 1a). The summertime peak value is about twice of the wintertime minimum value. This seasonal cycle points to natural sources of NO from microbial processes, i.e., nitrogen input from the melting of glaciers and permafrost as well as more vigorous microbial activity leading to NO emissions in warm seasons (Pilegaard, 2013; Wang et al., 2011). The surrounding areas of these natural lakes (population density < 8 km^{-2}) exhibit a similar seasonality in NO_2 VCDs (Figure 1b).

The differences in NO_2 VCDs between natural lakes and their surrounding areas also exhibit a seasonal variation (Figure 1c). In summer and autumn, the lake–surrounding differences are statistically significantly positive ($p < 0.01$) based on cross-lake Wilcoxon signed-rank test, indicating generally higher NO_2 VCDs over natural lakes than their surrounding areas. For summer specifically, individual-lake test based on paired lake–surrounding differences shows that 65 % of natural lakes exhibit statistically significantly higher NO_2 VCDs than their surrounding areas ($p < 0.05$ based on cross-year Wilcoxon signed-rank test); and that 92 % of natural lakes exhibit higher NO_2 VCDs than their surrounding areas (including statistically significant and insignificant cases). In winter and spring, nearly 67 % and 48 % of natural lakes exhibit lower NO_2 VCDs than their surrounding areas; and the median and mean NO_2 VCDs over all natural lakes are close to those over their surrounding areas (Table S3). These results indicate that lakes are the natural source of NO in warm seasons, and their emissions reach minimum values in winter due to weakened microbial activity and lake freezing in mid-to-high latitudes (Wang et al., 2022a).

To further verify that the NO_2 VCD signal and its seasonal pattern observed over natural lakes are from the lake, rather than the shoreline sources that could be contaminated by open fires and anthropogenic activities, we conduct a sensitivity test using only lake-interior grid cells (Sect. 2.8). The resulting NO_2 VCDs over natural lakes follow the aforementioned seasonal pattern (Figure S9), with 62 % of natural lakes exhibiting significantly higher NO_2 VCDs than their surrounding areas in summer ($p < 0.05$ based on Wilcoxon signed-rank test), and 91 % of natural lakes exhibit higher NO_2 VCDs than their surrounding areas (including statistically significant and insignificant cases).

Opposite to natural lakes, the 198 human-influenced lakes and their surrounding areas exhibit a peak of NO_2 VCDs in winter and a minimum in summer (Figure 1d and 1e). The wintertime peak value is about 1.4 times the summertime minimum. This seasonality is similar to that in urban areas, and is caused by a longer lifetime and higher anthropogenic emissions of NO in winter (Crippa et al., 2020; Shah et al., 2020). There are no statistically significant differences in NO_2 VCDs between human-influenced lakes and their surrounding areas in all seasons ($p > 0.1$ based on Wilcoxon signed-rank test, Figure 1f, Table S4). In addition, the human-influenced lakes exhibit higher NO_2

https://doi.org/10.5194/egusphere-2026-6515
Preprint. Discussion started: 9 November 2026
© Author(s) 2026. CC BY 4.0 License.

VCDs than the natural lakes in both winter (i.e., by a factor of about 4) and summer (by a factor of about 1.4), likely because of the contributions (in addition to natural emissions) from human activities on lakes such as shipping, sightseeing tours and aquaculture as well as atmospheric transport from human-influenced surrounding areas.

We further assess the potential influence of satellite air mass factor (AMF) calculation uncertainty, such as due to different aerosol treatments, on the observed lake enhancement by comparing the summer-averaged NO_2 VCDs from POMINO-TROPOMI (with explicit aerosol treatment) and official TM5-MP-DOMINO product (with implicit aerosol) over Asia (70°–140° E, 15°–55° N) in 2018–2024. For natural and human-influenced lakes, the NO_2 VCDs derived from POMINO-TROPOMI are slightly higher than those from the official product (5.8 % and 11.4 %, respectively) with strong correlation (0.93 and 0.99, respectively) (Figure S10). However, the lake-to-surrounding NO_2 VCD ratios agree even better between these two products (with difference of 1.6 % and 0.8 % and correction of 0.96 and 0.98 for the natural and human-influenced lakes, respectively) (Figure S10). These results suggest that the satellite VCD data are reliable for lake emission assessment.

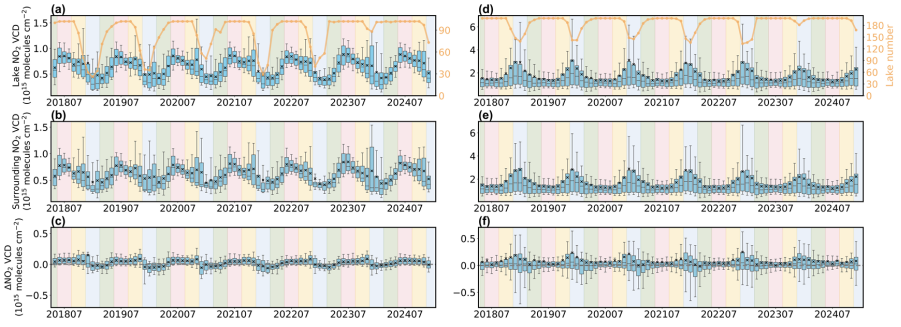


Figure 1. Monthly variation in NO_2 VCDs over lakes and surrounding areas in 2018–2024. (a, b) Monthly average NO_2 VCDs over 102 natural lakes and surroundings; **(c)** the difference in NO_2 VCDs between natural lakes and surroundings; **(d, e)** monthly average NO_2 VCDs over 198 human-influenced lakes and surroundings; **(f)** the difference in NO_2 VCDs between human-influenced lakes and surroundings. The yellow lines in **(a)** and **(d)** indicate the number of lakes with valid data. The green, pink, yellow and blue colors in the background denote spring, summer, autumn and winter, respectively. Each box represents the interquartile range (IQR), with the line inside indicating the median value and the cross indicating the mean value. Box whiskers extend to the 10th and 90th percentiles. VCDs data are from the POMINO research product for Asia and the official product for other regions.

3.2 NO emissions from lakes

Figure 2 and Figure 3 show the multi-year summer average early-afternoon emission intensities (per km^2 per hour) and total emissions (per hour) of NO from the 300 lakes in five continents (Sect. 2.7). It is obvious that NO emissions are widely

https://doi.org/10.5194/egusphere-2026-6515
Preprint. Discussion started: 9 November 2026
© Author(s) 2026. CC BY 4.0 License.

distributed across the NH lakes. The mean (± one standard deviation; same hereafter) emission intensity from all lakes reaches 0.15 ± 0.32 kg N km^{-2} h^{-1}, which is nearly four times larger than the summer early-afternoon soil NO emission intensity from croplands in the NH (0.03 ± 0.02 kg N km^{-2} h^{-1}) (Weng et al., 2020). The median emission intensity for these 300 lakes is about 0.10 kg N km^{-2} h^{-1}.

From the perspective of individual lakes, Figures S7 and S8 illustrate the spatial patterns of NO_2 VCDs, de-backgrounded NO_2 VCDs (i.e., after removing NO_2 in the free troposphere, Sect. 2.3), flux divergence, effective diffusion and NO emissions for three human-influenced lakes and three natural lakes with the highest emission intensities as examples. These figures show that the emissions of human-influenced lakes are comparable to those of the surrounding grid cells, and that natural lakes exhibit obvious NO_2 VCD and emission hotspots. Moreover, positive flux divergence is observed in both human-influenced and natural lakes, suggesting net outward transport of NO_2 from these lakes to their surroundings. Overall, these spatial patterns further demonstrate that both human-influenced and natural lakes act as local emission sources, rather than being solely influenced by transport from surrounding areas.

Almost all of the natural lakes (101 out of 102) are located in Asia and North America. Their emission intensities range from 0.03 to 0.28 kg N km^{-2} h^{-1}, exhibiting a slight right-skewed distribution with a mean value of 0.10 ± 0.06 kg N km^{-2} h^{-1} and a skewness (standardized 3rd central moment) of 1.06. This means the existence of high values, with the median (0.09 kg N km^{-2} h^{-1}) being slightly lower than the mean. About 97 % of these lakes exhibit emission intensities larger than 0.03 kg N km^{-2} h^{-1} (the average value for the NH cropland soil), and 14 % exhibit emission intensities larger than 0.15 kg N km^{-2} h^{-1}.

Compared with natural lakes, the 198 human-influenced lakes exhibit a much wider range of summertime NO emission intensities (0.03–5.38 kg N km^{-2} h^{-1}). The average emission intensity (0.17 ± 0.39 kg N km^{-2} h^{-1}) is 1.7 times of that for natural lakes, consistent with their higher NO_2 VCDs (Figure 1, Tables S2 and S3). This difference persists among the different continents, with the largest contrast occurring in Asia (by a factor of about 2.2). The emission intensity enhancement reflects that in human-influenced lakes, PHLET-derived emissions include the combined contributions of fuel combustions from aquaculture facilities and ships, as well as natural and human-influenced lake microbial processes. In particular, aquaculture and the inflow of nearby wastewater provide more nutrients and chemical reaction substrates for microorganisms (Dunne et al., 2021; Upadhyay et al., 2023). The emission intensities of human-influenced lakes exhibit a right-skewed distribution, similar to that for as natural lakes, but the skewness (11.91) is much greater due to the existence of extremely high values (up to 5.38 kg N km^{-2} h^{-1}). Thus, the median value (0.10 kg N km^{-2} h^{-1}) is much smaller than the mean.

As a sensitivity test, we recalculate lake NO emission intensities using only lake-interior grid cells (Sect. 2.8). This results in even higher average emission intensities, 0.15 ± 0.13 kg N km^{-2} h^{-1} for natural lakes and 0.18 ± 0.43 kg N km^{-2} h^{-1} for human-influenced lakes. This means that the derived lake NO emissions, particularly for natural lakes, are from the inner parts of lakes rather than along the lake shorelines (in

https://doi.org/10.5194/egusphere-2026-6515
Preprint. Discussion started: 9 November 2026
© Author(s) 2026. CC BY 4.0 License.

which case the estimated emissions could be contaminated by non-lake sources). This spatial pattern is also evident in the three exemplary lakes in Figure S8, where NO emissions are generally higher over the lake-interior grid cells than those over the shoreline-adjacent grid cells.

For human-influenced lakes, the emission intensities in Asia are higher than those in other continents. For example, seven out of the top 10 human-influenced lakes in terms of emission intensity are located in India and China (Figure 2b). Among them, Govind Ballabah Pant Sagar has the highest emission intensity (5.38 ± 1.25 kg N km^{-2} h^{-1}, Figure S7m). This lake is one of the biggest reservoirs in India, with tourism activities and six super thermal power plants (capacity ≥ 1000 MW) nearby. The associated human activities can alter the biological and chemical properties of the lake, which may in turn affect NO emissions.

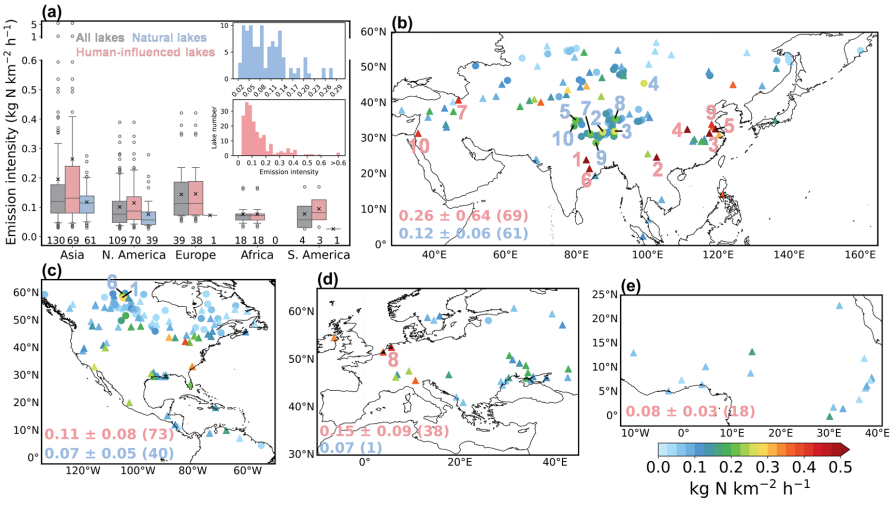


Figure 2. Multi-year summer average NO emission intensities from lakes in the Northern Hemisphere during 2018–2024. (a) Average emission intensities from lakes in each continent. Each box represents the IQR, with the line inside indicating the median value and the cross indicating the mean value. Box whiskers extend to the 10th and 90th percentiles, and the circles show data outside the 10th–90th percentile range. The numbers at the bottom represent the number of lakes in each box. The blue and red histograms inside illustrate the frequency distributions of emission intensities in natural lakes and human-influenced lakes, respectively. **(b–e)** Spatial distribution of emission intensities for individual lakes in Asia, North America and South America, Europe and Africa, respectively. Filled circles and triangles represent natural lakes and human-influenced lakes, respectively. The red and blue numbers indicate the top 10 lakes ranked by emission intensities in human-influenced lakes and natural lakes, respectively. The numbers in the lower left corner of each panel represent the mean ± std emission intensity, and the numbers in parentheses represent the number of lakes.

We multiply NO emission intensity by lake area to yield total emissions per hour for each lake in summer early afternoon (Figure 3). The total emissions from 300 lakes amount to 70.95 ± 13.98 Tons N h^{-1}, equivalent to twice the anthropogenic emissions

https://doi.org/10.5194/egusphere-2026-6515
Preprint. Discussion started: 9 November 2026
© Author(s) 2026. CC BY 4.0 License.

in Japan (33.17 Tons N h^{-1}) (Hoesly et al., 2018), 43 % of power-sector emissions in China (164.41 Tons N h^{-1}) (Li et al., 2017), or 15 % of soil emissions from croplands in the NH (470.34 Tons N h^{-1}) (Weng et al., 2020) in summer early afternoon; here, the diurnal variations of anthropogenic (Crippa et al., 2020) and soil (Weng et al., 2020) emissions based on previous work are accounted for. The lake total emissions are 10–35 times the shipping emissions for the same lakes reported in the CEDS (1.98 Tons N h^{-1}) and EDGAR (6.17 Tons N h^{-1}) inventories. Assuming that all lakes with an area exceeding 0.03 km^2 in the NH (0–60° N) (Pi et al., 2022), covering a total area of 1.6×10^6 km^2, have the median emission intensity derived here (0.10 kg N km^{-2} h^{-1}), they would emit 164.29 Tons N h^{-1} of NO in total, about 35 % of emissions from the NH croplands; and if the median emission intensity from the natural lakes (0.09 kg N km^{-2} h^{-1}) is used, the total natural emission from all NH lakes would amount to 140.64 Tons N h^{-1}, or 30 % of the NH croplands.

Among the 300 lakes, human-influenced and natural lakes contribute 92 % and 8 % to the NH total emission, respectively. The contribution of human-influenced lakes is much larger, as a combined result of more lake area (by a factor of 9.7) and higher emission intensities. Among the five continents, North America has the highest lake emission (56 %) due to the largest lake area (3.83×10^5 km^2, Figure S11). Asia comes second (31 %) because of its second largest lake area and the highest emission intensity. The emission contributions from Europe (9 %), Africa (3 %) and South America (0.3 %) are much smaller.

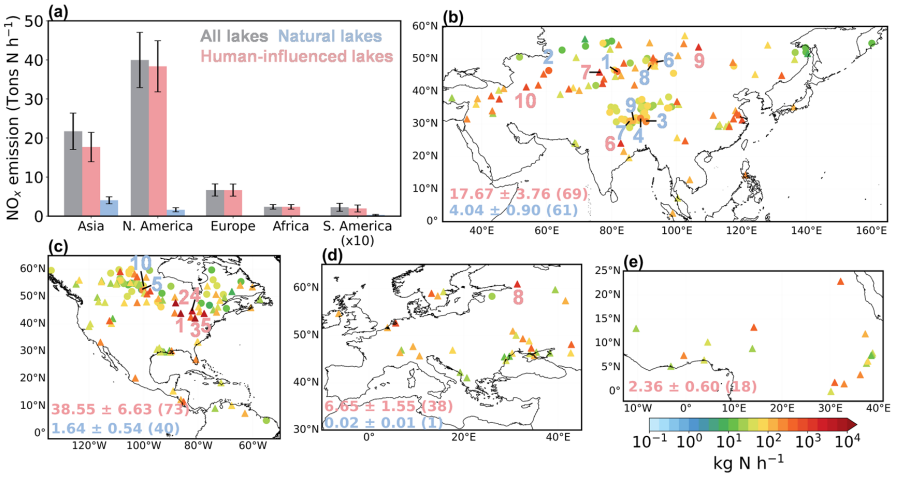


Figure 3. Multi-year summer average NO emission amounts from lakes in the Northern Hemisphere in 2018–2024. (a) Total NO emission amounts from lakes in each continent. The error bars indicate the emission uncertainty (± 1-σ). **(b–e)** Spatial distribution of NO emissions from individual lakes in Asia, North America and South America, Europe and Africa, respectively. Filled circles and triangles represent natural lakes and human-influenced lakes, respectively. The red and blue numbers indicate the top 10 lakes ranked by emission amounts in human-influenced lakes and natural lakes, respectively. The numbers in the lower left corner of each panel represent the total emissions ± uncertainty (Tons N h^{-1}), and the numbers in parentheses represent the number of lakes.

https://doi.org/10.5194/egusphere-2026-6515
Preprint. Discussion started: 9 November 2026
© Author(s) 2026. CC BY 4.0 License.

From 2018 to 2024, for both natural and human-influenced lakes, the interannual variability of lake-average emission intensity and total emissions is small with no statistically significant trend ($p > 0.1$ based on Mann–Kendall test, Figure S12). Given the relatively small interannual variability, a longer time series is needed to firmly determinate the trend of emission intensity, if any. Here, for each lake, the change in lake area after 2020 is not considered due to lack of data, but this is not expected to have a significant impact on the emission trend.

3.3 Top-10 emitting lakes

To better understand the importance of lake NO emissions, we compare the top 10 emitting human-influenced and natural lakes (labeled with red and blue numbers in Figure 3b–e) with 49 alpha cities. As lake NO emissions show only slight interannual variability, their multi-year average values during 2018–2024 are analyzed here. These 49 cities are economic hubs linking their respective regions or states with the world economy, as designated by the Globalization and World Cities Research Network (GAWC) (Taylor and Derudder, 2015). Anthropogenic emissions of these alpha cities in summer early afternoon are taken from two bottom-up global emission inventories including CEDS v202504 (Hoesly et al., 2018) and EDGAR v8.1 (Crippa et al., 2024), with the diurnal variations based on EDGAR (Crippa et al., 2020). The emissions for each city are presented in Supplementary Data.

Figure 4a compares NO emissions from the top 10 emitting human-influenced lakes with 2018–2023 summer early-afternoon anthropogenic emissions of alpha cities from CEDS. The five Great Lakes in North America have the highest emissions due to their large lake area. Among them, Lake Michigan has the largest emission, which is lower than emissions of five alpha cities (São Paulo, Buenos Aires, Shanghai, Beijing and Riyadh) but higher than other 44 cities. Apart from the five Great Lakes, other five top-10 human-influenced lakes have emission amounts comparable to the highly-emitting cities such as Istanbul, Mexico and Seoul. In addition, Figure 4b shows that among the top 10 emitting natural lakes, Lake Alakol in Kazakhstan has the highest emission that is close to the level of Chicago. Other nine highest emitting natural lakes are comparable to many alpha cities such as Taipei, Houston and Paris. The total emissions of 102 natural lakes are close to Guangzhou and higher than 43 alpha cities.

Considering the uncertainty in CEDS, we further compare lake emissions with 2018–2022 summer early-afternoon anthropogenic emissions of 49 alpha cities from EDGAR. We find that lake emissions are also comparable to emissions of alpha cities in EDGAR (Figure S13). These results suggest that globally, lakes are a major source of NO emissions that cannot be ignored. Such NO emissions from lakes into the atmosphere should be included in numerical models to assess their impacts on tropospheric chemistry, climate and the nitrogen cycle.

https://doi.org/10.5194/egusphere-2026-6515
Preprint. Discussion started: 9 November 2026
© Author(s) 2026. CC BY 4.0 License.

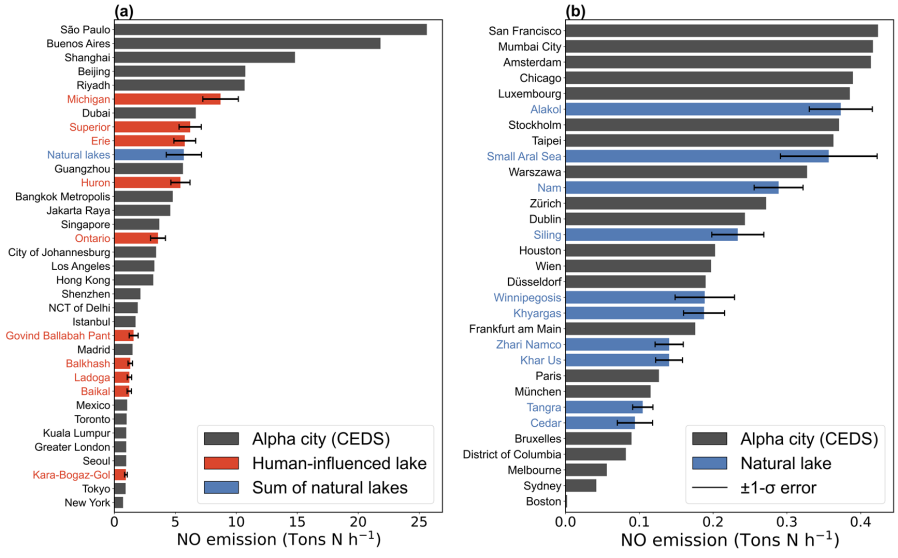


Figure 4. Comparison of NO emissions from lakes and alpha cities in summer early afternoon. **(a)** Comparison between emissions of the top 10 emitting human-influenced lakes and anthropogenic emissions of alpha cities. The total emission from all natural lakes is also shown. **(b)** Comparison between emissions of the top 10 emitting natural lakes and anthropogenic emissions of alpha cities. Anthropogenic emissions of cities are derived from multi-year average of the CEDS inventory in 2018–2023.

3.4 Environmental factors affecting cross-lake emission variability

We further investigate potential factors of lake environment that might affect NO emission intensities. Following previous work on lake GHG emissions (DelSontro et al., 2018; Marotta et al., 2014; Yang et al., 2025; Zhou et al., 2021) and given the data availability, we select two factors with data available for global lakes (i.e., lake surface temperature (LST) and dissolved oxygen (DO)) and three other factors with data available for a limited number of lakes (i.e., lake total nitrogen (TN), total phosphorus (TP), and Chl-a). We focus on how these lake factors are spatially associated with NO emission intensities.

For LST and DO, we examine the cross-lake relationships between them and the lake-average emission intensity. Previous work on inland water N_2O emissions have shown that higher temperatures increase microbial activity, and hypoxic conditions promote anaerobic denitrification processes, thereby increasing the emissions (Yang et al., 2023a; Yang et al., 2025). We find that across the 102 natural lakes, there is a strong negative correlation between DO and NO emission intensity ($r = -0.38$, $p = 0.00$, Figure S14). For LST, there is also a statistically significant negative correlation with NO emission intensity across the 102 lakes ($r = -0.21$, $p = 0.04$). This apparent negative LST-NO relationship is because of the 38 high-altitude, low-temperature but highly-emitting lakes on the Tibetan Plateau, compared with other lakes outside the plateau. In

https://doi.org/10.5194/egusphere-2026-6515
Preprint. Discussion started: 9 November 2026
© Author(s) 2026. CC BY 4.0 License.

fact, positive correlations exist between LST and NO emission intensity among these Tibetan Plateau lakes (r = 0.21, p = 0.21) and among other 62 mid-latitude (30° N–60° N) lakes (r = 0.21, p = 0.10). For the human-influenced lakes, lake NO emission intensities are significantly positively correlated with LST (r = 0.32, p = 0.00) and negatively correlated with DO (r = -0.15, p = 0.04, Figure S15).

For TN, TP and Chl-a, in situ measurements (Naderian et al., 2024) are available in 35 grid cells in 15 lakes, 40 grid cells in 15 lakes, and 183 grid cells in 35 lakes, respectively, after excluding those grid cells directly influenced by anthropogenic emission sources such as shipping and aquaculture. As key eutrophic substances in lakes (Conley et al., 2009), nitrogen and phosphorus can enhance the productivity of phytoplankton (Xu et al., 2009) and increase the content of organic matter and the substrates for nitrification and denitrification processes (Duan et al., 2025; Liu et al., 2018). In addition, under anoxic conditions, ammonium produced by organic matter decomposition and nitrite produced by nitrification and nitrate reduction may support anaerobic ammonium oxidation (anammox), another important nitrogen-loss pathway in which NO serves as a key metabolic intermediate (Kartal et al., 2011; Zhang et al., 2022). Chl-a is an important indicator of algal biomass and primary productivity in lakes. For the grid cells with in situ data, after logarithmic transformation, NO emission intensities are positively correlated with TN (r = 0.38, p = 0.02), TP (r = 0.70, p = 0.00) and Chl-a (r = 0.34, p = 0.00) (Figure S16), indicating that higher nutrient levels in lakes are more favorable for NO emissions.

Previous studies have suggested that N_2O in lakes is produced through microbially mediated nitrification and denitrification. The relationships between lake NO emission intensity and LST, DO, TN, TP and Chl-a are broadly similar to those observed for N_2O (DelSontro et al., 2018; Yang et al., 2023b; Yang et al., 2025), suggesting that these two nitrogen oxides may be influenced by common environmental and biogeochemical controls. These factors can affect microbial activity and nutrient availability, thereby influencing aquatic nitrogen cycling and potentially regulating NO production.

4 Summary and Implication

As a key player in the nitrogen cycle, NO can be emitted from many anthropogenic and natural processes, yet accurate characterization and quantification of different emission sources remain difficult. With the reduction of on-land anthropogenic NO emissions such as power generation and transportation in many regions, other emission sources are becoming increasingly important (Lu et al., 2021; Tan et al., 2023; Zhao et al., 2025). However, there are still knowledge gaps and uncertainties regarding these sources. Taking advantage of high-resolution satellite NO_2 observations and an advanced algorithm for emission quantification, here we reveal considerable NO emissions from 300 large lakes in the NH. The average lake emission intensity is nearly four times greater than the summer early-afternoon soil emission intensity from croplands in the NH. Emissions from many individual lakes are comparable to global alpha cities, and the total emissions from all lakes are equivalent to twice anthropogenic emissions in Japan or nearly half of power-sector emissions in China. These previously

https://doi.org/10.5194/egusphere-2026-6515
Preprint. Discussion started: 9 November 2026
© Author(s) 2026. CC BY 4.0 License.

overlooked or poorly-represented emissions might have played important roles in nitrogen deposition, atmospheric chemistry forming ozone and $PM_{2.5}$, and climate change.

Both anthropogenic activities and natural processes contribute to lake NO emissions. Lake NO emission intensities are related to environmental factors (e.g., LST, DO, TN, TP and Chl-a) in similar ways with N_2O emissions (DelSontro et al., 2018; Yang et al., 2023b; Yang et al., 2025), suggesting that microbial processes may play an important role in lake NO emissions in addition to N_2O. Besides microbial processes, previous studies have proposed that the photolysis of nitrite in the open ocean surface can also produce NO (Tian et al., 2024; Tian et al., 2020). Given the limited measurements in lakes, especially natural lakes, further research is needed to determine the exact processes and mechanisms of lake NO emissions such as nitrification, denitrification, anammox and nitrite photolysis, and how the environmental factors specifically cause the spatiotemporal variability in lake emission intensity. These processes and factors are often sensitive to climate conditions, thus ongoing climate change (e.g., rising temperature, changing precipitation, permafrost thawing, nitrogen input alteration, and nutrient change) are modulating NO emissions from lakes. For anthropogenic emissions from lakes, the current bottom-up inventories are subject to inadequacies and inaccuracies in activity data (e.g., on lake shipping, tourism, and aquaculture) and emission factors. Efforts to improve data collection and harmonization will help reduce the uncertainty in emission estimation. Combining satellite observations, in situ measurements, emission statistics and model simulations will be necessary to fully understand the mechanisms of lake NO emissions and their feedback with climate and aquatic systems. To this end, our study offers the first spaceborne quantitative picture of NO emissions from lakes across the Northern Hemisphere.

Data availability

NO_2 VCD and NO emission data produced in this study are available in Supplementary Data. The official TM5-MP-DOMINO Level 2 product are available at https://sentinels.copernicus.eu/data-products. POMINO-TROPOMI Level 2 product are available at https://www.pku-atmos-acm.org/acmProduct.php/#TROPOMI. GSOCmap data are available at https://data.apps.fao.org/glosis. SoilGrids data are available at https://files.isric.org/soilgrids/latest. Global Energy Monitor (GEM) data are obtained from https://globalenergymonitor.org/. Other data obtained from publicly available sources are available from the references.

Acknowledgements

This research is supported by the National Natural Science Foundation of China (grant no. 42430603), the National Key Research and Development Program of China (grant no. 2023YFC3705802), and the National Key Scientific and Technological Infrastructure project “Earth System Numerical Simulation Facility” (EarthLab). AI is used to facilitate the conversion of QDOAS from C++ to Python.

https://doi.org/10.5194/egusphere-2026-6515
Preprint. Discussion started: 9 November 2026
© Author(s) 2026. CC BY 4.0 License.

Author contributions

J.L. conceived the research. J.L. and W.T. designed the research. W.T. performed the research. H.K. and S.W. helped construct the PHLET algorithm. T.D. and M.V.R provided the original C++ code of QDOAS. M.W. helped reimplement the original code of QDOAS in Python and conduct NO_2 retrievals. M.W. and Y.Z. helped interpret satellite NO_2 data. L.B. helped obtain ECMWF real-time analysis wind field data. Y.L., D.W., L.F., X.W. and K.S. commented on the analysis on NO emissions versus environmental factors. Y.C. provided the unpublished in situ NO_2 concentration measurements for Lake Taihu. W.T. and J.L. analyzed the results and wrote the paper with comments from other authors.

Competing interests

Some authors are members of the editorial board of Atmospheric Chemistry and Physics. The authors declare no other competing interests.

Additional information

Extended data for this paper provided below.

Supplementary information

Supplementary_Information.docx includes Supplementary Figures 1–16 and Tables 1–4.

Supplementary_Data.xlsx includes detailed information of NO_2 VCDs and NO emissions from the 300 lakes, and the anthropogenic emissions of 49 alpha cities from two bottom-up emission inventories.

Correspondence and requests for materials should be addressed to Jintai Lin.

References

Beaulieu, J. J., DelSontro, T., and Downing, J. A.: Eutrophication will increase methane emissions from lakes and impoundments during the 21st century, Nature Communications, 10, 10.1038/s41467-019-09100-5, 2019.

Byun, D. and Schere, K. L.: Review of the Governing Equations, Computational Algorithms, and Other Components of the Models-3 Community Multiscale Air Quality (CMAQ) Modeling System, Applied Mechanics Reviews, 59, 51-77, 10.1115/1.2128636, 2006.

Cerdeiro, D., Komaromi, A., Liu, Y., and Saeed, M.: World Seaborne Trade in Real Time: A Proof of Concept for Building AIS-based Nowcasts from Scratch, IMF Working Papers, 2020, 10.5089/9781513544106.001, 2020.

Chen, Z., Li, R., Raza, S. T., Rene, E. R., Xie, P., and Liu, Y.: Environment-specific fluorescence probe for investigating the detection mechanism of nitric oxide in lakes, Journal of Hazardous Materials, 494, 10.1016/j.jhazmat.2025.138622, 2025.

Clark, D. R., Ferguson, R. M. W., Harris, D. N., Matthews Nicholass, K. J., Prentice, H. J., Randall, K.

https://doi.org/10.5194/egusphere-2026-6515
Preprint. Discussion started: 9 November 2026
© Author(s) 2026. CC BY 4.0 License.

C., Randell, L., Warren, S. L., and Dumbrell, A. J.: Streams of data from drops of water: 21st century molecular microbial ecology, WIREs Water, 5, 10.1002/wat2.1280, 2018.

Conley, D. J., Paerl, H. W., Howarth, R. W., Boesch, D. F., Seitzinger, S. P., Havens, K. E., Lancelot, C., and Likens, G. E.: Controlling Eutrophication: Nitrogen and Phosphorus, Science, 323, 1014-1015, 10.1126/science.1167755, 2009.

Crippa, M., Guizzardi, D., Pagani, F., Schiavina, M., Melchiorri, M., Pisoni, E., Graziosi, F., Muntean, M., Maes, J., Dijkstra, L., Van Damme, M., Clarisse, L., and Coheur, P.: Insights into the spatial distribution of global, national, and subnational greenhouse gas emissions in the Emissions Database for Global Atmospheric Research (EDGAR v8.0), Earth System Science Data, 16, 2811-2830, 10.5194/essd-16-2811-2024, 2024.

Crippa, M., Solazzo, E., Huang, G., Guizzardi, D., Koffi, E., Muntean, M., Schieberle, C., Friedrich, R., and Janssens-Maenhout, G.: High resolution temporal profiles in the Emissions Database for Global Atmospheric Research, Scientific Data, 7, 10.1038/s41597-020-0462-2, 2020.

Darmenov, A. S. and Silva, A. d.: The Quick Fire Emissions Dataset (QFED): Documentation of versions 2.1, 2.2 and 2.4, 2015.

DelSontro, T., Beaulieu, J. J., and Downing, J. A.: Greenhouse gas emissions from lakes and impoundments: Upscaling in the face of global change, Limnology and Oceanography Letters, 3, 64-75, 10.1002/lol2.10073, 2018.

Donaldson, D. J.: Sailboat Measurements of Trace Gases in Urban Environments: In Toronto, Canada, Ground-Level NO2 Is Consistently Elevated over Lake Ontario versus at the Shoreline, but O3 Is Not, ACS Earth and Space Chemistry, 10, 1543-1553, 10.1021/acsearthspacechem.6c00049, 2026.

Duan, Z., Liang, J., Shi, L., Xu, Y., Gao, W., and Tan, X.: Eutrophication Heterogeneously Enhances Organic Matter and Phosphorus Exchanges among Dissolved, Particulate, and Sedimentary Phases in a Large Shallow Lake, Environmental Science & Technology, 59, 13264-13274, 10.1021/acs.est.4c12091, 2025.

Duarte, C. M. and Prairie, Y. T.: Prevalence of Heterotrophy and Atmospheric CO_2 Emissions from Aquatic Ecosystems, Ecosystems, 8, 862-870, 10.1007/s10021-005-0177-4, 2005.

Dunne, A., Carvalho, S., Morán, X. A. G., Calleja, M. L., and Jones, B.: Localized effects of offshore aquaculture on water quality in a tropical sea, Marine Pollution Bulletin, 171, 10.1016/j.marpolbul.2021.112732, 2021.

Dunne, J. P., Horowitz, L. W., Adcroft, A. J., Ginoux, P., Held, I. M., John, J. G., Krasting, J. P., Malyshev, S., Naik, V., Paulot, F., Shevliakova, E., Stock, C. A., Zadeh, N., Balaji, V., Blanton, C., Dunne, K. A., Dupuis, C., Durachta, J., Dussin, R., Gauthier, P. P. G., Griffies, S. M., Guo, H., Hallberg, R. W., Harrison, M., He, J., Hurlin, W., McHugh, C., Menzel, R., Milly, P. C. D., Nikonov, S., Paynter, D. J., Ploshay, J., Radhakrishnan, A., Rand, K., Reichl, B. G., Robinson, T., Schwarzkopf, D. M., Sentman, L. T., Underwood, S., Vahlenkamp, H., Winton, M., Wittenberg, A. T., Wyman, B., Zeng, Y., and Zhao, M.: The GFDL Earth System Model Version 4.1 (GFDL‐ESM 4.1): Overall Coupled Model Description and Simulation Characteristics, Journal of Advances in Modeling Earth Systems, 12, 10.1029/2019ms002015, 2020.

Eyth, A., Seltzer, K., Vukovich, J., Farkas, C., Godfrey, J., Dayton, L., and Dietrich, Y.: Technical Support Document (TSD): Preparation of Emissions Inventories for the 2022v2 North American Emissions Modeling Platform, U.S. Environmental Protection Agency, Research Triangle Park, NC, Technical Support Document EPA-454/B-25-002, 2025.

Fayt, C., Danckaert, T., Van Roozendael, M., and Vlietinck, J.: QDOAS trace gas retrieval software

https://doi.org/10.5194/egusphere-2026-6515
Preprint. Discussion started: 9 November 2026
© Author(s) 2026. CC BY 4.0 License.



(3.7.12), Royal Belgian Institute for Space Aeronomy [code], 10.18758/oqvqk2j3, 2026.

Global Energy Monitor: Global Cement and Concrete Tracker (July 2026 release), Global Energy Monitor [dataset], 2026a.

Global Energy Monitor: Global Coal Plant Tracker (July 2026 release), Global Energy Monitor [dataset], 2026b.

Global Energy Monitor: Global Iron and Steel Tracker (June 2026 (V1) release), Global Energy Monitor [dataset], 2026c.

Global Energy Monitor: Global Oil and Gas Extraction Tracker (March 2026 release), Global Energy Monitor [dataset], 2026d.

Global Energy Monitor: Global Oil and Gas Plant Tracker (August 2026 release), Global Energy Monitor [dataset], 2026e.

Guenther, A. B., Jiang, X., Heald, C. L., Sakulyanontvittaya, T., Duhl, T., Emmons, L. K., and Wang, X.: The Model of Emissions of Gases and Aerosols from Nature version 2.1 (MEGAN2.1): an extended and updated framework for modeling biogenic emissions, Geoscientific Model Development, 5, 1471-1492, 10.5194/gmd-5-1471-2012, 2012.

Hoesly, R. M., Smith, S. J., Feng, L., Klimont, Z., Janssens-Maenhout, G., Pitkanen, T., Seibert, J. J., Vu, L., Andres, R. J., Bolt, R. M., Bond, T. C., Dawidowski, L., Kholod, N., Kurokawa, J.-i., Li, M., Liu, L., Lu, Z., Moura, M. C. P., O'Rourke, P. R., and Zhang, Q.: Historical (1750–2014) anthropogenic emissions of reactive gases and aerosols from the Community Emissions Data System (CEDS), Geoscientific Model Development, 11, 369-408, 10.5194/gmd-11-369-2018, 2018.

Huang, T., Zhu, X., Zhong, Q., Yun, X., Meng, W., Li, B., Ma, J., Zeng, E. Y., and Tao, S.: Spatial and Temporal Trends in Global Emissions of Nitrogen Oxides from 1960 to 2014, Environmental Science & Technology, 51, 7992-8000, 10.1021/acs.est.7b02235, 2017.

Johnson, M. S., Matthews, E., Du, J., Genovese, V., and Bastviken, D.: Methane Emission From Global Lakes: New Spatiotemporal Data and Observation - Driven Modeling of Methane Dynamics Indicates Lower Emissions, Journal of Geophysical Research: Biogeosciences, 127, 10.1029/2022jg006793, 2022.

Kaiser, J. W., Heil, A., Andreae, M. O., Benedetti, A., Chubarova, N., Jones, L., Morcrette, J. J., Razinger, M., Schultz, M. G., Suttie, M., and van der Werf, G. R.: Biomass burning emissions estimated with a global fire assimilation system based on observed fire radiative power, Biogeosciences, 9, 527-554, 10.5194/bg-9-527-2012, 2012.

Kartal, B., Maalcke, W. J., de Almeida, N. M., Cirpus, I., Gloerich, J., Geerts, W., Op den Camp, H. J., Harhangi, H. R., Janssen-Megens, E. M., Francoijs, K. J., Stunnenberg, H. G., Keltjens, J. T., Jetten, M. S., and Strous, M.: Molecular mechanism of anaerobic ammonium oxidation, Nature, 479, 127-130, 10.1038/nature10453, 2011.

Kay, S., Hedley, J. D., and Lavender, S.: Sun Glint Correction of High and Low Spatial Resolution Images of Aquatic Scenes: a Review of Methods for Visible and Near-Infrared Wavelengths, Remote Sensing, 1, 697-730, 10.3390/rs1040697, 2009.

Khandelwal, A., Karpatne, A., Ravirathinam, P., Ghosh, R., Wei, Z., Dugan, H. A., Hanson, P. C., and Kumar, V.: ReaLSAT, a global dataset of reservoir and lake surface area variations, Scientific Data, 9, 10.1038/s41597-022-01449-5, 2022.

Kong, H., Lin, J., Chen, L., Zhang, Y., Yan, Y., Liu, M., Ni, R., Liu, Z., and Weng, H.: Considerable Unaccounted Local Sources of NO_x Emissions in China Revealed from Satellite, Environmental Science & Technology, 56, 7131-7142, 10.1021/acs.est.1c07723, 2022.

Kong, H., Lin, J., Ni, R., Du, M., Wang, J., Chen, L., Xu, C., Yan, Y., Weng, H., and Zhang, Y.: Satellite

https://doi.org/10.5194/egusphere-2026-6515
Preprint. Discussion started: 9 November 2026
© Author(s) 2026. CC BY 4.0 License.

detected weak decline of nitrogen oxides emissions in economically small cities of China, Environmental Research Letters, 20, 10.1088/1748-9326/ade170, 2025.

Kong, H., Lin, J., Tang, G., Zhang, Y., Li, C., Xu, C., Shen, L., Liu, X., Yang, K., Su, H., Xu, W., and Tan, W.: Reply to: NO_2 satellite retrievals biased by absorption in water, Nature Geoscience, 17, 976-978, 10.1038/s41561-024-01546-7, 2024.

Kong, H., Lin, J., Zhang, Y., Li, C., Xu, C., Shen, L., Liu, X., Yang, K., Su, H., and Xu, W.: High natural nitric oxide emissions from lakes on Tibetan Plateau under rapid warming, Nature Geoscience, 16, 474-477, 10.1038/s41561-023-01200-8, 2023.

Kurokawa, J. and Ohara, T.: Long-term historical trends in air pollutant emissions in Asia: Regional Emission inventory in ASia (REAS) version 3, Atmospheric Chemistry and Physics, 20, 12761-12793, 10.5194/acp-20-12761-2020, 2020.

Labzovskii, L. D., van Geffen, J., Liu, M., van der A, R., de Laat, J., Leune, B., Eskes, H., Lin, X., Ding, J., and Richter, A.: NO_2 satellite retrievals biased by absorption in water, Nature Geoscience, 17, 972-975, 10.1038/s41561-024-01545-8, 2024.

Li, M., Liu, H., Geng, G., Hong, C., Liu, F., Song, Y., Tong, D., Zheng, B., Cui, H., Man, H., Zhang, Q., and He, K.: Anthropogenic emission inventories in China: a review, National Science Review, 4, 834-866, 10.1093/nsr/nwx150, 2017.

Li, Y., Tian, H., Yao, Y., Shi, H., Bian, Z., Shi, Y., Wang, S., Maavara, T., Lauerwald, R., and Pan, S.: Increased nitrous oxide emissions from global lakes and reservoirs since the pre-industrial era, Nature Communications, 15, 10.1038/s41467-024-45061-0, 2024.

Liu, D., Zhong, J., Zheng, X., Fan, C., Yu, J., and Zhong, W.: N_2O Fluxes and Rates of Nitrification and Denitrification at the Sediment–Water Interface in Taihu Lake, China, Water, 10, 10.3390/w10070911, 2018.

Liu, L., Yang, J., Yu, Z., and Wilkinson, D. M.: The biogeography of abundant and rare bacterioplankton in the lakes and reservoirs of China, The ISME Journal, 9, 2068-2077, 10.1038/ismej.2015.29, 2015.

Liu, M., Lin, J., Kong, H., Boersma, K. F., Eskes, H., Kanaya, Y., He, Q., Tian, X., Qin, K., Xie, P., Spurr, R., Ni, R., Yan, Y., Weng, H., and Wang, J.: A new TROPOMI product for tropospheric NO_2 columns over East Asia with explicit aerosol corrections, Atmospheric Measurement Techniques, 13, 4247-4259, 10.5194/amt-13-4247-2020, 2020.

Liu, Y. and Whitman, W. B.: Metabolic, Phylogenetic, and Ecological Diversity of the Methanogenic Archaea, Annals of the New York Academy of Sciences, 1125, 171-189, 10.1196/annals.1419.019, 2008.

Lu, X., Ye, X., Zhou, M., Zhao, Y., Weng, H., Kong, H., Li, K., Gao, M., Zheng, B., Lin, J., Zhou, F., Zhang, Q., Wu, D., Zhang, L., and Zhang, Y.: The underappreciated role of agricultural soil nitrogen oxide emissions in ozone pollution regulation in North China, Nature Communications, 12, 10.1038/s41467-021-25147-9, 2021.

Marotta, H., Pinho, L., Gudasz, C., Bastviken, D., Tranvik, L. J., and Enrich-Prast, A.: Greenhouse gas production in low-latitude lake sediments responds strongly to warming, Nature Climate Change, 4, 467-470, 10.1038/nclimate2222, 2014.

Messager, M. L., Lehner, B., Grill, G., Nedeva, I., and Schmitt, O.: Estimating the volume and age of water stored in global lakes using a geo-statistical approach, Nature Communications, 7, 10.1038/ncomms13603, 2016.

Muñoz Sabater, J.: ERA5-Land hourly data from 1950 to present., Copernicus Climate Change Service (C3S) Climate Data Store (CDS). 10.24381/cds.e2161bac 2019.

Naderian, D., Noori, R., Heggy, E., Bateni, S. M., Bhattarai, R., Nohegar, A., and Sharma, S.: A water

https://doi.org/10.5194/egusphere-2026-6515
Preprint. Discussion started: 9 November 2026
© Author(s) 2026. CC BY 4.0 License.

quality database for global lakes, Resources, Conservation and Recycling, 202, 10.1016/j.resconrec.2023.107401, 2024.

Paolo, F. S., Kroodsma, D., Raynor, J., Hochberg, T., Davis, P., Cleary, J., Marsaglia, L., Orofino, S., Thomas, C., and Halpin, P.: Satellite mapping reveals extensive industrial activity at sea, Nature, 625, 85-91, 10.1038/s41586-023-06825-8, 2024.

Pi, X., Luo, Q., Feng, L., Xu, Y., Tang, J., Liang, X., Ma, E., Cheng, R., Fensholt, R., Brandt, M., Cai, X., Gibson, L., Liu, J., Zheng, C., Li, W., and Bryan, B. A.: Mapping global lake dynamics reveals the emerging roles of small lakes, Nature Communications, 13, 10.1038/s41467-022-33239-3, 2022.

Pilegaard, K.: Processes regulating nitric oxide emissions from soils, Philosophical Transactions of the Royal Society B: Biological Sciences, 368, 10.1098/rstb.2013.0126, 2013.

Preena, P. G., Rejish Kumar, V. J., and Singh, I. S. B.: Nitrification and denitrification in recirculating aquaculture systems: the processes and players, Reviews in Aquaculture, 13, 2053-2075, 10.1111/raq.12558, 2021.

Raymond, P. A., Hartmann, J., Lauerwald, R., Sobek, S., McDonald, C., Hoover, M., Butman, D., Striegl, R., Mayorga, E., Humborg, C., Kortelainen, P., Dürr, H., Meybeck, M., Ciais, P., and Guth, P.: Global carbon dioxide emissions from inland waters, Nature, 503, 355-359, 10.1038/nature12760, 2013.

Savvichev, A. S., Babenko, V. V., Lunina, O. N., Letarova, M. A., Boldyreva, D. I., Veslopolova, E. F., Demidenko, N. A., Kokryatskaya, N. M., Krasnova, E. D., Gaisin, V. A., Kostryukova, E. S., Gorlenko, V. M., and Letarov, A. V.: Sharp water column stratification with an extremely dense microbial population in a small meromictic lake, Trekhtzvetnoe, Environmental Microbiology, 20, 3784-3797, 10.1111/1462-2920.14384, 2018.

Shah, V., Jacob, D. J., Li, K., Silvern, R. F., Zhai, S., Liu, M., Lin, J., and Zhang, Q.: Effect of changing NO_x lifetime on the seasonality and long-term trends of satellite-observed tropospheric NO_2 columns over China, Atmospheric Chemistry and Physics, 20, 1483-1495, 10.5194/acp-20-1483-2020, 2020.

Soued, C., del Giorgio, P. A., and Maranger, R.: Nitrous oxide sinks and emissions in boreal aquatic networks in Québec, Nature Geoscience, 9, 116-120, 10.1038/ngeo2611, 2015.

Stanier, C. O., Pierce, R. B., Abdi-Oskouei, M., Adelman, Z. E., Al-Saadi, J., Alwe, H. D., Bertram, T. H., Carmichael, G. R., Christiansen, M. B., Cleary, P. A., Czarnetzki, A. C., Dickens, A. F., Fuoco, M. A., Hughes, D. D., Hupy, J. P., Janz, S. J., Judd, L. M., Kenski, D., Kowalewski, M. G., Long, R. W., Millet, D. B., Novak, G., Roozitalab, B., Shaw, S. L., Stone, E. A., Szykman, J., Valin, L., Vermeuel, M., Wagner, T. J., Whitehill, A. R., and Williams, D. J.: Overview of the Lake Michigan Ozone Study 2017, Bulletin of the American Meteorological Society, 102, E2207-E2225, 10.1175/bams-d-20-0061.1, 2021.

Tan, W., Wang, H., Su, J., Sun, R., He, C., Lu, X., Lin, J., Xue, C., Wang, H., Liu, Y., Liu, L., Zhang, L., Wu, D., Mu, Y., and Fan, S.: Soil Emissions of Reactive Nitrogen Accelerate Summertime Surface Ozone Increases in the North China Plain, Environmental Science & Technology, 57, 12782-12793, 10.1021/acs.est.3c01823, 2023.

Taylor, P. and Derudder, B.: World City Network, 10.4324/9781315730950, 2015.

Tian, Y., Gong, J.-C., Liu, C.-Y., Zhang, J., Li, P.-F., and Yang, G.-P.: The Ocean Serves as a Net Source of Atmospheric Nitric Oxide but a Net Sink of Nitrogen Dioxide, Environmental Science & Technology, 58, 21662-21668, 10.1021/acs.est.4c10709, 2024.

Tian, Y., Xue, C., Liu, C.-Y., Yang, G.-P., Li, P.-F., Feng, W.-H., and Bange, H. W.: Nitric oxide (NO) in the Bohai Sea and the Yellow Sea, Biogeosciences, 16, 4485-4496, 10.5194/bg-16-4485-2019, 2019.

Tian, Y., Yang, G.-P., Liu, C.-Y., Li, P.-F., Chen, H.-T., and Bange, H. W.: Photoproduction of nitric oxide in seawater, Ocean Science, 16, 135-148, 10.5194/os-16-135-2020, 2020.

https://doi.org/10.5194/egusphere-2026-6515
Preprint. Discussion started: 9 November 2026
© Author(s) 2026. CC BY 4.0 License.

Upadhyay, P., Prajapati, S. K., and Kumar, A.: Impacts of riverine pollution on greenhouse gas emissions: A comprehensive review, Ecological Indicators, 154, 10.1016/j.ecolind.2023.110649, 2023.

van Geffen, J., Eskes, H., Sneep, M., ter Linden, M., and Veefkind, J. P.: Improved NO2 spectral fits for TROPOMI and OMI by removing wavelengths around 430 nm, Atmospheric Measurement Techniques, 19, 4233-4254, 10.5194/amt-19-4233-2026, 2026.

Veefkind, J. P., Aben, I., McMullan, K., Förster, H., de Vries, J., Otter, G., Claas, J., Eskes, H. J., de Haan, J. F., Kleipool, Q., van Weele, M., Hasekamp, O., Hoogeveen, R., Landgraf, J., Snel, R., Tol, P., Ingmann, P., Voors, R., Kruizinga, B., Vink, R., Visser, H., and Levelt, P. F.: TROPOMI on the ESA Sentinel-5 Precursor: A GMES mission for global observations of the atmospheric composition for climate, air quality and ozone layer applications, Remote Sensing of Environment, 120, 70-83, 10.1016/j.rse.2011.09.027, 2012.

Wang, F., Lin, W., Wang, J., and Zhu, T.: NO_x Release from Snow and Ice Covered Surface in Polar Regions and the Tibetan Plateau, Advances in Climate Change Research, 2, 141-148, 10.3724/sp.J.1248.2011.00141, 2011.

Wang, M., Lin, J., Zhang, Y., Jin, X., Tan, W., Kong, H., and Wang, S.: Satellite Retrieval of Tropospheric NO2 under Fire Conditions, EGUsphere [preprint], 10.5194/egusphere-2026-2410, 2026.

Wang, X., Feng, L., Qi, W., Cai, X., Zheng, Y., Gibson, L., Tang, J., Song, X. p., Liu, J., Zheng, C., and Bryan, B. A.: Continuous Loss of Global Lake Ice Across Two Centuries Revealed by Satellite Observations and Numerical Modeling, Geophysical Research Letters, 49, 10.1029/2022gl099022, 2022a.

Wang, Z., Zhang, J., Yang, X., Huang, C., Su, F., Liu, X., Liu, Y., and Zhang, Y.: Global mapping of the landside clustering of aquaculture ponds from dense time-series 10 m Sentinel-2 images on Google Earth Engine, International Journal of Applied Earth Observation and Geoinformation, 115, 10.1016/j.jag.2022.103100, 2022b.

Weng, H., Lin, J., Martin, R., Millet, D. B., Jaeglé, L., Ridley, D., Keller, C., Li, C., Du, M., and Meng, J.: Global high-resolution emissions of soil NO_x, sea salt aerosols, and biogenic volatile organic compounds, Scientific Data, 7, 10.1038/s41597-020-0488-5, 2020.

Wiedinmyer, C., Kimura, Y., McDonald-Buller, E. C., Emmons, L. K., Buchholz, R. R., Tang, W., Seto, K., Joseph, M. B., Barsanti, K. C., Carlton, A. G., and Yokelson, R.: The Fire Inventory from NCAR version 2.5: an updated global fire emissions model for climate and chemistry applications, Geoscientific Model Development, 16, 3873-3891, 10.5194/gmd-16-3873-2023, 2023.

WorldPop and Center for International Earth Science Information Network (CIESIN), C. U.: Global High Resolution Population Denominators Project - Funded by The Bill and Melinda Gates Foundation (OPP1134076) [dataset], 10.5258/SOTON/WP00647, 2018.

Xiao, Q., Hu, Z., Fu, C., Bian, H., Lee, X., Chen, S., and Shang, D.: Surface nitrous oxide concentrations and fluxes from water bodies of the agricultural watershed in Eastern China, Environmental Pollution, 251, 185-192, 10.1016/j.envpol.2019.04.076, 2019.

Xu, C., Lin, J., Wang, S., Kong, H., Zhang, Y., Yun, Y., Ren, F., Wang, M., Tan, W., Wang, J., Bai, L., and Gao, J.: Satellite-detected nitrogen oxides emission changes from power plant dynamics in North China, Environmental Research Letters, 21, 10.1088/1748-9326/ae860b, 2026.

Xu, H., Paerl, H. W., Qin, B., Zhu, G., and Gaoa, G.: Nitrogen and phosphorus inputs control phytoplankton growth in eutrophic Lake Taihu, China, Limnology and Oceanography, 55, 420-432, 10.4319/lo.2010.55.1.0420, 2009.

Yang, C., Du, W. J., He, R.-L., Hu, Y.-R., Liu, H., Huang, T., and Li, W.-W.: Spatiotemporal Patterns of

https://doi.org/10.5194/egusphere-2026-6515
Preprint. Discussion started: 9 November 2026
© Author(s) 2026. CC BY 4.0 License.



Methane and Nitrous Oxide Emissions in China's Inland Waters Identified by Machine Learning Technique, ACS ES&T Water, 4, 936-947, 10.1021/acsestwater.3c00064, 2023a.

Yang, F., Sun, C., Wang, H., Hu, X., Wang, S., Zhang, M., Zhang, L., and Zhong, J.: Significant spatiotemporal variability of nitrous oxide emissions from a temperate reservoir experiencing intensive aquaculture disturbance, Agriculture, Ecosystems & Environment, 348, 10.1016/j.agee.2023.108427, 2023b.

Yang, F., Zheng, X., Yao, E., Wang, D., Chang, S., Huang, W., Zhang, L., Wang, J., and Zhong, J.: N_2O emissions from a multi-habitat lake: Patterns and controls, Journal of Hydrology, 658, 10.1016/j.jhydrol.2025.133209, 2025.

Zhang, D., Li, M., Yang, Y., Yu, H., Xiao, F., Mao, C., Huang, J., Yu, Y., Wang, Y., Wu, B., Wang, C., Shu, L., He, Z., and Yan, Q.: Nitrite and nitrate reduction drive sediment microbial nitrogen cycling in a eutrophic lake, Water Res, 220, 118637, 10.1016/j.watres.2022.118637, 2022.

Zhang, Y., Lin, J., Kim, J., Lee, H., Park, J., Hong, H., Van Roozendael, M., Hendrick, F., Wang, T., Wang, P., He, Q., Qin, K., Choi, Y., Kanaya, Y., Xu, J., Xie, P., Tian, X., Zhang, S., Wang, S., Cheng, S., Cheng, X., Ma, J., Wagner, T., Spurr, R., Chen, L., Kong, H., and Liu, M.: A research product for tropospheric NO2 columns from Geostationary Environment Monitoring Spectrometer based on Peking University OMI NO2 algorithm, Atmospheric Measurement Techniques, 16, 4643-4665, 10.5194/amt-16-4643-2023, 2023.

Zhang, Y., Shi, K., Woolway, R. I., Wang, X., and Zhang, Y.: Climate warming and heatwaves accelerate global lake deoxygenation, Science Advances, 11, 10.1126/sciadv.adt5369, 2025.

Zhao, Y., Nielsen, C. P., Lei, Y., McElroy, M. B., and Hao, J.: Quantifying the uncertainties of a bottom-up emission inventory of anthropogenic atmospheric pollutants in China, Atmospheric Chemistry and Physics, 11, 2295-2308, 10.5194/acp-11-2295-2011, 2011.

Zhao, Y., Su, Z., Chen, Y., Hou, S., Lu, X., Zheng, B., Liu, L., Pan, Y., Xu, W., Liu, X., and Zhang, L.: Rising importance of agricultural nitrogen oxide emissions in China's future PM2.5 pollution mitigation, npj Climate and Atmospheric Science, 8, 10.1038/s41612-025-00976-3, 2025.

Zhou, Y., Xu, X., Song, K., Yeerken, S., Deng, M., Li, L., Riya, S., Wang, Q., and Terada, A.: Nonlinear pattern and algal dual-impact in N_2O emission with increasing trophic levels in shallow lakes, Water Res, 203, 117489, 10.1016/j.watres.2021.117489, 2021.